PCCP

PAPER

View Article Online
View Journal | View Issue

Cite this: *Phys. Chem. Chem. Phys.*, 2019, **21**, 6868

Quantum state control on the chemical reactivity of a transition metal vanadium cation in carbon dioxide activation

Yih Chung Chang, † Yuntao Xu † and Cheuk-Yiu Ng *

By combining a newly developed two-color laser pulsed field ionization-photoion (PFI-PI) source and a double-quadrupole–double-octopole (DQDO) mass spectrometer, we investigated the integral cross sections (σs) of the vanadium cation (V^+) toward the activation of CO_2 in the center-of-mass kinetic energy (E_{cm}) range from 0.1 to 10.0 eV. Here, V^+ was prepared in single spin–orbit levels of its lowest electronic states, a^5D_J (J = 0–4), a^5F_J (J = 1–5), and a^3F_J (J = 2–4), with well-defined kinetic energies. For both product channels VO^+ + CO and VCO^+ + O identified, $V^+(a^3F_{2,3})$ is found to be greatly more reactive than $V^+(a^5D_{0,2})$ and $V^+(a^5F_{1,2})$, suggesting that the V^+ + CO_2 reaction system mainly proceeds *via* a "weak quintet-to-triplet spin-crossing" mechanism favoring the conservation of total electron spins. In addition, no J-state dependence was observed. The distinctive structures of the quantum electronic state selected integral cross sections observed as a function of E_{cm} and the electronic state of the V^+ ion indicate that the difference in the chemical reactivity of the title reaction originated from the quantum-state instead of energy effects. Furthermore, this work suggests that the selection of the quantum electronic states a^3F_J (J = 2–4) of the transition metal V^+ ion can greatly enhance the efficiency of CO_2 activation.

Received 29th January 2019,
Accepted 8th March 2019

DOI: 10.1039/c9cp00575g

rsc.li/pccp

I. Introduction

Transition metal (TM) cations play indispensable roles in many fields,[1–4] particularly in organometallic chemistry and catalysis. The intrinsic electronic structures of TM cations, which result from interactions of valence electrons residing in partially filled d or f orbitals, are responsible for their distinct chemical reactivity. These interactions give rise to dense manifolds of low-lying quantum electronic states with a variety of spin multiplicities, making the fundamental understanding of the chemical reactivity of TM cations more difficult.[5] It has long been recognized that to better unravel the complex chemistry of TM cations involved, it is necessary to perform chemical reactivity or integral cross section (σ) measurements of ion–molecule collisions with TM cations prepared in single quantum electronic states as well as in high kinetic energy resolution.[6–9] Recently, efforts have been made to develop novel experimental techniques to cool ions down to ultracold temperatures[10,11] for cold ion–molecule reaction studies. However, these cold ion experiments mainly focused on preparing ions in the ground state. Due to the experimental challenge, σ measurements with TM cations prepared in single excited quantum states have not been realized.

By implementing a laser ablation metal source for the production of supersonically cooled TM atoms with a two-color laser excitation scheme for pulsed field ionization-photoion (PFI-PI) detection, we were successful in developing a quantum state selected ion source for TM cations, achieving high intensity and well-defined kinetic energy resolution.[12,13] This novel experimental scheme can be viewed as a continuation of the vacuum ultraviolet (VUV) PFI-PI technique developed in our laboratory which has been employed previously for σ measurements involving quantum-state-selected reactant ions of $N_2^+(X^2\Sigma_g^+: v^+ = 0–2; N^+ = 0–9)$,[14–18] $H_2O^+(X^2B_1: v_1^+v_2^+v_3^+ = 000, 020, 100; N^+_{Ka+Kc+} = 0_{00}–3_{22})$,[19–22] $H_2^+(X^2\Sigma_g^+: v^+ = 1–3; N^+ = 0–3)$,[23] $O_2^+(a^4\Pi_{u5/2,3/2,1/2,-1/2}: v^+ = 1–2; J^+)$,[24] and $O_2^+(X^2\Pi_{g3/2,1/2}: v^+ = 22–23; J^+)$.[24] Recently, this newly developed two-color laser PFI-PI ion source has been successfully employed to prepare vanadium cations (V^+) in thirteen spin–orbit coupled quantum electronic states, a^5D_J (J = 0–4), a^5F_J (J = 1–5), and a^3F_J (J = 2–4), where J is the quantum number of the total angular momentum from spin–orbit coupling. When this PFI-PI ion source is coupled to a double-quadrupole–double-octopole (DQDO) mass spectrometer, quantum-state-selected σ measurements of ion–molecule reactions involving $V^+(a^5D_{0–4}$, $a^5F_{1–5}$, and $a^3F_{2–4})$ become possible. As pointed out previously, based on the parity

Department of Chemistry, University of California, Davis, Davis, CA 95616, USA. E-mail: cyng@ucdavis.edu

† These two authors contribute equally to this work.

and electron spin selection rules, the radiative lifetimes of these electronic states are expected to be significantly longer than that of the experimental measurement cycle of about 100 μs.[25–27]

Activation of carbon dioxide (CO_2) has become one of the most popular research subjects in both energy and environmental studies, due to its almost exponentially increased emission as a result of anthropogenic activities in the past century, and notoriously high thermodynamic stability and kinetic inertness.[28,29] One of the key strategies for CO_2 activation is to discover suitable reactants that can enhance the activation efficiency of CO_2, and TM cations are known to be among the promising candidates for this purpose.[30–32] As early as 1981, Staley *et al.* studied the oxidation reactions between TM cations and neutral molecules including CO_2, utilizing ion cyclotron resonance mass spectrometry. More interestingly, they found that V^+ did not react with CO_2.[30] Since 1995, by employing a guided-ion beam mass spectrometer, Armentrout and co-workers carried out a series of investigations on the activation of CO_2 with many TM cations. In particular, in their study of the $V^+ + CO_2$ reaction, V^+ ions were mainly prepared in the ground electronic state $V^+(a^5D_J)$.[31] Three reaction channels were observed leading to the formation of VO^+, VCO^+, and VO_2^+. Reactivity enhancement for the $V^+ + CO_2$ reaction was observed by raising the electron beam energy used for V^+ ion preparation, suggesting that the chemical reactivity of the excited electronic states of the V^+ ion is significantly higher than that of the ground state. However, due to uncertainties of the state distributions of V^+ ions and the lack of precise state identifications, the reactivity of V^+ in individual excited electronic states cannot be deciphered unambiguously. In 2006, Bohme *et al.* published a systematic study on the reaction rate constant measurements of CO_2 with atomic TM cations mainly prepared in their ground electronic states, aiming for the study of room-temperature kinetics and trends in reactivity.[27] One year later, Davico *et al.* reported on a similar chemical kinetics study of reactions between TM cations and CO_2.[32] Interestingly, both experiments showed no reaction between $V^+(a^5D_J)$ and CO_2. This conclusion could be ascribed to the very low chemical reactivity of the $V^+(a^5D_J) + CO_2$ reaction, and the possible low detection sensitivity of these experiments.

As mentioned above, previous ion–molecule reaction studies on the chemical reactivity of TM cations toward CO_2 were conducted with TM cations mainly prepared in their ground states,[27,31] or a variety mixtures of ground and excited electronic states, where the identities of excited states were often not clearly known.[31,32] As a result, little quantitative information on the activation of CO_2 has been reported with TM cations (including V^+) populated in their excited electronic states. To our best knowledge, no experimental work has been reported on the spin–orbit or J state dependence of chemical reactivity for TM cations due to the same reason. In this work, we report for the first time, the successful measurements of the chemical reactivity of the reactions $V^+(a^5D_J, a^5F_J, \text{and } a^3F_J) + CO_2$ as a function of not only E_{cm}, but also the quantum spin–orbit electronic state of the V^+ ion.

II. Experimental considerations

The experimental arrangement and procedures used in the two-color laser PFI-PI ion source and the PFI-PI double-quadrupole–double-octopole (DQDO) ion–molecule reaction apparatus have been described in detail previously.[12–15] Thus, only a brief description is given below.

Coupling of the laser ablation metal beam source with two-color laser PFI-PI detection

Neutral precursor gaseous V atoms are generated from a rotating V rod by laser ablation. The plumes of plasma and gaseous neutral species thus formed are carried forward and cooled down by collision with a synchronized pulsed He beam through supersonic expansion. The charged species that remain in the V/He beam are effectively removed by applying a DC electric field downstream right after the supersonic expansion. As pointed out previously, ion lenses E1, I1, and I2 are the most essential components of the ion source. The V/He supersonic beam is skimmed by two conical skimmers before entering the photoexcitation (PEX) region, which is defined by the spacing between ion lenses E1 and I1.

The neutral V atom beam thus formed are then excited to high-n ($n \geq 70$) Rydberg states at the PEX center by employing a two-color laser excitation scheme. Two dye lasers are pumped by the second or third harmonic output from one identical Nd-YAG laser operating at 30 Hz. The output from the first dye laser VIS (ω_1) is fixed at 457.845 nm, allowing the excitation of the V atom to the neutral intermediate state $V[3d^3(^4F)4s4p(^3P^\circ), z^4G_{5/2}{}^\circ]$ from the neutral $V(3d^34s^2\ a^4F_{3/2})$ ground state. The output of the second dye laser UV(ω_2) provides a scanning range of 307.288–239.904 nm, which excites the V atom from the $V[3d^3(^4F)4s4p(^3P^\circ), z^4G_{5/2}{}^\circ]$ intermediate state to the high-n Rydberg states of the V atom which are several wavenumbers below the ionization thresholds of the quantum spin–orbit coupled electronic states, $V^+(a^5D_J, a^5F_J, \text{and } a^3F_J)$.

Besides the formation of neutral high-n Rydberg V species [V*(n)], prompt ions are also produced by direct photoionization as well as autoionization, which are not state-selected ions and usually populate in a variety of ion internal states. The next step is to separate prompt ions from the V*(n) species. In order to do this, a pulsed separation electric field (amplitude = 2 V cm^{-1}, duration = 2.0 μs) is applied on lens I1 to retard the prompt ions at a delay of 150 ns with respect to the laser photoexcitation. The positively charged prompt ions retarded by the separation field will move backwards relatively to the direction of the pulsed neutral V atom beam, while the neutral excited V*(n) species that survived the separation field will continue to travel forward along the supersonic beam direction. Thus, the spatial separation of neutral V*(n) from prompt ions can be achieved by using a sufficiently high separation or retardation field.

The final step is the generation of V^+ cations in the selected single spin–orbit coupled quantum electronic states without contamination by prompt ions. To achieve this, a second pulsed electric field (amplitude = 41.7 V cm^{-1} and duration = 0.75 μs)

is applied on lens E1 immediately after the separation field on lens I1 is switched off. This electric field pulse serves as the Stark electric field for ionizing neutral excited V*(n) atoms to form V^+ PFI-PIs, as well as extracting state-selected PFI-PIs formed out of the PEX region. The short duration (0.75 μs) of the PFI pulse used is the key factor for obtaining a narrow kinetic energy spread of V^+ PFI-PI ions. Since the PFI-PI field is turned off before any of the V^+ PFI-PIs exit the PEX region, all the V^+ PFI-PIs are expected to gain the same kinetic energies. The prompt ions are also extracted by the PFI field. However, the prompt ions have kinetic energies lower than those of the V^+ PFI-PIs. Thus, by applying an appropriate potential barrier on lens I2, the prompt ions can be completely rejected, while only V^+ PFI-PI ions are permitted to pass through lens I2 to enter the reaction gas cell.

PFI-PI DQDO ion–molecule reaction apparatus and σ measurements

The PFI-PI DQDO ion–molecule reaction apparatus consists of, in sequential order, a laser ablation supersonic PFI-PI V^+ ion source, a reactant quadrupole mass filter (QMF), a dc quadrupole ion bender equipped with a microchannel plate (MCP) ion detector, a reaction gas cell situated between two rf-octopole ion guides which are powered by the same radio frequency power supply, a product QMF, and a Daly-type ion detector. The reactant QMF in this experiment is only used as an ion lens. The DC quadrupole ion bender together with the MCP ion detector is located near the entrance of the radio frequency (rf)-octopole ion guides. The DC quadrupole ion bender together with the MCP detector, when coupled with the Daly-type ion detector situated at the exit of the product QMF, makes transmission evaluation of the ion beam possible. The quantum state selected V^+ ions are guided by the rf-octopole to enter the gas cell, where reactions with CO_2 occur. The effective length of the gas cell used is 5.6 cm, and the typical CO_2 pressure used in the gas cell is 2.0×10^{-4} Torr as monitored using a MKS Baratron. All product ions together with unreacted V^+ PFI-PI ions are collected and guided by the rf-octopole to enter the product QMF for mass analysis and ion intensity measurements. The intensities of the reactant and product ions measured using the Daly-type ion detector are used for integral cross section measurements.

Specifically, σ measurements are carried out by comparing the relative intensities of the reactant and product ions. Based on the thin target ion-neutral scattering scheme to deduce absolute cross sections, $\sigma = [(kT)/(Pl)][\ln((I + i)/I)]$, where k, T, P, l, I, and i represent the Boltzmann constant, the temperature and the pressure of the neutral reactant in the reactant gas cell, the effective length of the gas cell, the intensity of the unreacted reactant V^+ ions, and the intensity of the product ions, respectively. The σ values determined in the present study are the average of at least three independent measurements. The run-to-run uncertainty is in the range of 5–15%. The error limits for absolute σ values are estimated to be about 30%.

In addition, the E_{cm} is converted from the laboratory kinetic energy (E_{lab}) by using the formula $E_{cm} = E_{lab}\,[M/(m^+ + M)]$, where m^+ and M represent the masses of the V^+ ion and the CO_2 molecule, respectively. As pointed out in previous studies,[33] in an ion beam-gas cell study, such as this one, the thermal motions of neutral CO_2 molecules in the reaction gas cell can be the main contribution to the spread of E_{cm} (ΔE_{cm}), especially in the low E_{cm} range. For the reaction of $V^+ + CO_2$, the estimated uncertainties for E_{cm} = 0.1, 0.5, 1.0, and 4.0 eV are 0.1, 0.3, 0.4 and 0.8 eV, respectively. The ΔE_{cm} spread can have an effect on smoothening structures of the $\sigma(E_{cm})$ curves, and the general trends for the $\sigma(E_{cm})$ curves are not expected to be greatly affected.

It should also be noted that the purity of the CO_2 sample used in the present work is 99.5%, even though it has a limited impact on the results of the present work. The 0.5% impurity is equivalent to 1×10^{-6} Torr in the gas cell since the pressure of CO_2 is controlled at 2×10^{-4} Torr for the present work. If all the impurity is O_2, based on the measured $\sigma(VO^+)$ values for $V^+ + O_2$ (to be published), the relative small values of $\sigma(a^5D_0\text{: } VO^+)$ and $\sigma(a^5F_1\text{: } VO^+)$ shown in Fig. 2(b) become even smaller, especially when $E_{cm} \leq 1.0$ eV. The largest effect may make $\sigma(a^5D_0\text{: } VO^+)$ and $\sigma(a^5F_1\text{: } VO^+)$ at E_{cm} = 0.1 eV smaller by about 25%. In contrast, this change on $\sigma(a^3F_2\text{: } VO^+)$ is within the uncertainty range. Therefore, we conclude that the effect on the results of this work from the impurity of the neutral CO_2 sample is limited.

III. Results and discussion

Mass spectra

Fig. 1(a) and (b) show the mass spectra of $V^+(a^3F_2)$ PFI-PIs without and with CO_2 filled in the gas cell, respectively. As shown in the black spectrum in Fig. 1(a), two peaks are observed at mass-to-charge (m/z) ratios of 51 and 67, which are assigned correspondingly to V^+ and VO^+. In order to view more clearly the mass spectrum in the m/z range above 51, the ion intensity is amplified by a factor of 10, together with shifting the baseline of the spectrum upward by 25, resulting in the red spectrum depicted in Fig. 1(a). The VO^+ ions observed here, mainly due to the inevitable oxidized layer on the surface of the V metal rod, can be considered as background ions. When CO_2 is filled into the reaction gas cell, three peaks are observed in Fig. 1(b) at m/z = 51, 67, and 79, which are assigned to V^+, VO^+, and VCO^+, respectively. Compared to those in Fig. 1(a), the V^+ peak is smaller and the VO^+ peak becomes much enhanced in Fig. 1(b), due to the reaction of $V^+ + CO_2$. In addition, a minor VCO^+ peak is observed in Fig. 1(b), representing a new reaction channel. For the measurements of both spectra shown in Fig. 1(a) and (b), the kinetic energies are controlled at E_{cm} = 5.0 eV. We note that no VO_2^+ ion is observed with V^+ prepared in all the three electronic states in the E_{cm} range of 0.1–10.0 eV for this reaction system. However, in one of the previous studies with V^+ prepared mainly in the ground electronic state,[31] the formation of VO_2^+ was reported with $\sigma(VO_2^+) < 2 \times 10^{-2}$ Å^2 at $E_{cm} > 9.0$ eV. Due to the very low $\sigma(VO_2^+)$ values and the high endothermicity, this product channel is unlikely to play any significant role in most chemical environments.

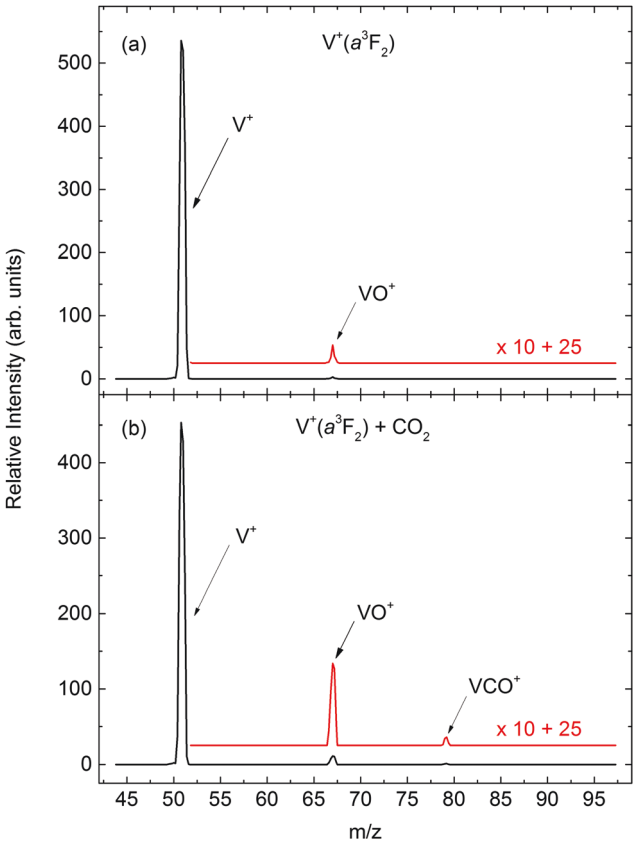

Fig. 1 Comparison of the mass spectra of (a) only $V^+(a^3F_2)$ and (b) $V^+(a^3F_2)$ with CO_2 filled in the gas cell. For (a), two peaks are observed at m/z = 51 and 67, which are assigned to V^+ and VO^+, respectively; and for (b), three peaks are observed at m/z = 51, 67, and 79, which are assigned to V^+, VO^+, and VCO^+, respectively. For both (a) and (b), the original spectra are shown in black curves, and the magnified ones (multiplied by 10 and then shifted up by 25) are shown in red for peaks with lower intensities. For both (a) and (b), the E_{cm} values are set at 5.0 eV.

Therefore, as shown in the mass spectra discussed above, two reaction product channels are observed leading to the formation of VO^+ + CO and VCO^+ + O, as listed in reactions (1) and (2) below along with their thermochemistry:[31,34,35]

$$V^+(a^5D_0) + CO_2(X^1\Sigma_g^+) \rightarrow VO^+(X^3\Sigma^-) + CO(X^1\Sigma^+)$$
$$\Delta E = -0.5 \pm 0.1 \text{ eV} \quad (1)$$

$$\rightarrow VCO^+(X^5\Delta) + O(^3P)\ \Delta E = 4.3 \pm 0.1 \text{ eV} \quad (2)$$

The heat of reaction (ΔE) is obtained with all reactants and products in their ground state. The heat of formation of VO^+ and VCO^+ is obtained based on the known bond energies of V^+–O and V^+–CO.[31,36] The ΔE values for the V^+ ion prepared in the other two excited quantum electronic states can be obtained by using the corresponding known electronic energies.[37]

Quantum electronic state dependence

Fig. 2(a) and (b) [Fig. 2(c) and (d)] show the σ curves for the formation of VO^+ [VCO^+] with V^+ prepared exclusively in each of the a^5D_0, a^5F_1, and a^3F_2 electronic states in the E_{cm} range from 0.1 to 10.0 eV. In particular, Fig. 2(a) [Fig. 2(c)] shows

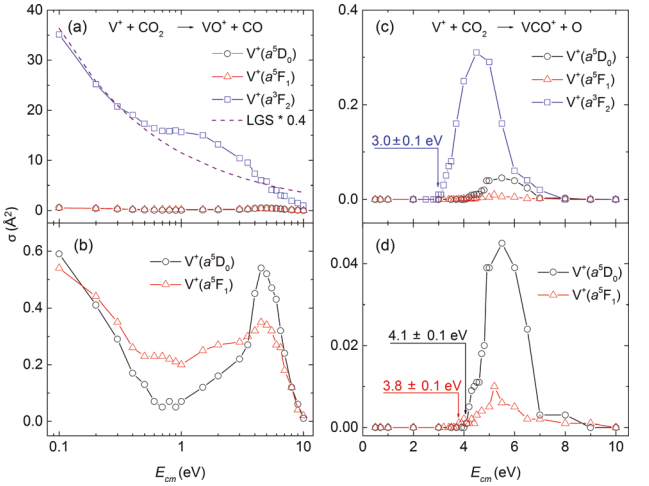

Fig. 2 Comparisons of (a) the $\sigma(a^5D_0$: $VO^+)$, $\sigma(a^5F_1$: $VO^+)$, and $\sigma(a^3F_2$: $VO^+)$ curves; (b) the magnified views of the $\sigma(a^5D_0$: $VO^+)$ and $\sigma(a^5F_1$: $VO^+)$ curves; (c) the $\sigma(a^5D_0$: $VCO^+)$, $\sigma(a^5F_1$: $VCO^+)$, and $\sigma(a^3F_2$: $VCO^+)$ curves; and (d) the magnified views of the $\sigma(a^5D_0$: $VCO^+)$ and $\sigma(a^5F_1$: $VCO^+)$ curves. The σ(LGS) curve (scaled by a factor of 0.4) calculated based on the LGS model is also shown as the purple dashed curve in the figure. All experimental σ curves were measured in the E_{cm} range of 0.1–10.0 eV. The run-to-run uncertainties are in the range of ± 5–15%.

comparison of $\sigma(a^5D_0$: $VO^+)$, $\sigma(a^5F_1$: $VO^+)$, and $\sigma(a^3F_2$: $VO^+)$ [$\sigma(a^5D_0$: $VCO^+)$, $\sigma(a^5F_1$: $VCO^+)$, and $\sigma(a^3F_2$: $VCO^+)$] curves, and Fig. 2(b) [Fig. 2(d)] shows a magnified view of the $\sigma(a^5D_0$: $VO^+)$ and $\sigma(a^5F_1$: $VO^+)$ [$\sigma(a^5D_0$: $VCO^+)$ and $\sigma(a^5F_1$: $VCO^+)$] curves, which are included at the bottom of Fig. 2(a) [Fig. 2(c)]. For each of the above three quantum electronic states, we have also examined the spin–orbit coupled J-state dependence, and no dependence on the J-state is found (see the Spin–orbit-state or J-state dependence section below).

One of the salient features of Fig. 2(a) is that $\sigma(a^5D_0$: $VO^+)$ and $\sigma(a^5F_1$: $VO^+)$ are much lower than $\sigma(a^3F_2$: $VO^+)$ by at least 10 times. More specifically, $\sigma(a^5D_0$: $VO^+)$ and $\sigma(a^5F_1$: $VO^+)$ at E_{cm} = 0.1, 1.0, 4.5, and 10.0 eV are about 60, 80, 10, and 50 times smaller than $\sigma(a^3F_2$: $VO^+)$, respectively. Such a drastic inhibition observed for $\sigma(a^5D_0$: $VO^+)$ and $\sigma(a^5F_1$: $VO^+)$ indicates that the reactant V^+ ions in quintet electronic states a^5D_0 and a^5F_1 are much less reactive toward CO_2 than that in the triplet electronic state a^3F_2. This behavior can be ascribed to a "weak spin-crossing" mechanism between the quintet and triplet reaction surfaces. The electron spins of reactant CO_2 and product CO in their ground electronic quantum states are zero. The lowest excited electronic state $CO(a^3\Pi)$ is 6.01 eV higher than the $CO(X^1\Sigma^+)$ ground state,[38] and thus, the formation of $CO(a^3\Pi)$ in the E_{cm} range of interest here can likely be ignored. Therefore, if the total electron spin is conserved along the reaction pathway, or the Wigner–Witmer spin-conservation rule[39] holds, the electron spin of the product VO^+ ion should be the same as that of the reactant V^+ ion. Both previous experimental and theoretical studies[36,40–42] have shown that the VO^+ ion has a triplet ground electronic state $X^3\Sigma^-$, and the lowest quintet electronic state $VO^+(a^5\Sigma^-)$ is about 3.3 eV higher in energy.[36] Thus, in order to form the product $VO^+(X^3\Sigma^-)$ ion

with the reactant V^+ ion in the quintet state, quintet-to-triplet "spin crossing" is needed, allowing the quintet reactant surface to "switch" into a triplet product surface. Based on the observation that $V^+(a^3F_2)$ is much more reactive, the surmised multiplicity of the favored intermediate should be triplet formed by the insertion of V^+ into the C–O bond of CO_2. This preference is consistent with previous theoretical calculations, which predicted that the triplet inserted $[OV^+CO]$ structure is exothermic and more stable than the quintet linear $[V^+OCO]$ intermediate.[43] The much smaller $\sigma(a^5D_0: VO^+)$ and $\sigma(a^5F_1: VO^+)$ compared to $\sigma(a^3F_2: VO^+)$ indicate that the efficiency of the "spin-crossing" is very low. From this point of view, the reaction system of $V^+ + CO_2$ mainly follows the reaction surface with the same spin multiplicity by obeying the Wigner–Witmer spin-conservation rule, *i.e.*, it behaves mostly nonadiabatically.[44]

This weak quintet-to-triplet spin-crossing reaction mechanism is illustrated schematically in the energy diagram of Fig. 3, constructed based on the heat of formation scale. On the left side of this figure, the reactant states $V^+(a^5D_0) + CO_2$, $V^+(a^5F_1) + CO_2$, and $V^+(a^3F_2) + CO_2$ are depicted as black (quintet) and red (triplet) lines. In the middle are two possible reaction intermediates $[V^+OCO]$ and $[OV^+CO]$, and on the right side, the product channels are depicted in red, black, or blue lines depending on their multiplicities. It is clear that a quintet-to-triplet "spin-crossing" mechanism is required for a reactant state with quintet multiplicity to form a product state with triplet multiplicity, as shown schematically by the purple dashed line in Fig. 3. Thus, the weak quintet-to-triplet spin-crossing serves as a "bottleneck" of the reaction, leading to the low reactivity for $V^+(a^5D_0)$ and $V^+(a^5F_1)$. In addition, when E_{cm} is high enough, more product channels become energetically accessible and spin-allowed: (1) the onset

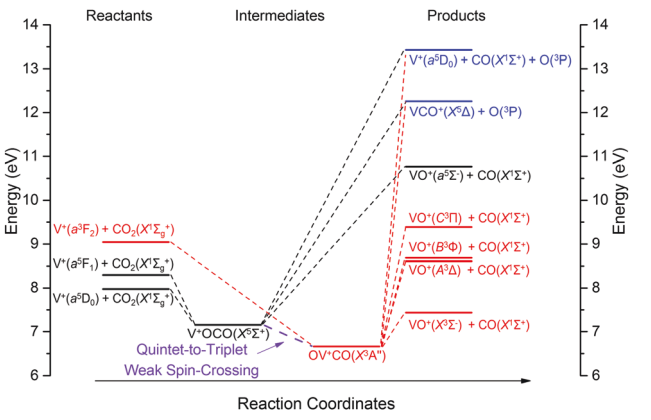

Fig. 3 Schematic energy level diagram of the $[V^+ + CO_2]$ reaction system in the heat-of-formation scale.[31,34,35,43] The left side shows the reactant states, $V^+(a^5D_0) + CO_2$ (black line), $V^+(a^5F_1) + CO_2$ (black line), and $V^+(a^3F_2) + CO_2$ (red line); the intermediates based on theoretical calculations[43] are shown in the middle of the figure, where the less preferred quintet intermediate $[V^+OCO]$ is highlighted in black and the preferred triplet intermediate $[OV^+CO]$ is shown in red. Possible product channels are depicted on the right side highlighted in red, black, or blue lines based on their multiplicities. The weak quintet-to-triplet spin-crossing is shown schematically along the reaction coordinates by the purple dashed line connecting the $[V^+OCO]$ and $[OV^+CO]$ intermediates in the middle.

of the "bump" observed for $\sigma(a^3F_2: VO^+)$ at $E_{cm} \approx 0.4$–0.5 eV in Fig. 2(a) may be indicative of the opening of product channel $VO^+(C^3\Pi) + CO\ (X^1\Sigma^+)$; (2) both $\sigma(a^5D_0: VO^+)$ and $\sigma(a^5F_1: VO^+)$ are expected to be enhanced when $VO^+(a^5\Sigma^-) + CO\ (X^1\Sigma^+)$ is opened up, which is seen in Fig. 2(b); and (3) both $\sigma(VO^+)$ and $\sigma(VCO^+)$ are observed to decrease when E_{cm} reaches 4.5–5.5 eV as shown in Fig. 2(b)–(d). This decrease can be ascribed to the opening of the collision-induced dissociation channel to form $V^+(a^5D_0) + CO(X^1\Sigma^+) + O(^3P)$. Thus, invoking a "weak quintet-to-triplet spin-crossing" mechanism can account for the significantly lower $\sigma(a^5D_0: VO^+)$ and $\sigma(a^5F_1: VO^+)$ compared to $\sigma(a^3F_2: VO^+)$.

Similar quantum electronic state effects on the VO^+ product channel are also observed for the VCO^+ product channel. As shown in Fig. 2(c) and (d), $\sigma(VCO^+)$ has much smaller values ($<10\%$) than $\sigma(VO^+)$ discussed above, partly due to the high endothermicity of the VCO^+ channel. The peak $\sigma(a^3F_2: VCO^+)$ value is about one order of magnitude higher than that of $\sigma(a^5D_0: VCO^+)$, which in turn is about 5 times higher than that of $\sigma(a^5F_1; VCO^+)$, indicating again that the triplet electronic state $V^+(a^3F_2)$ is significantly more reactive toward CO_2 than the two quintet states. Similarly, the observed inhibition of $\sigma(a^5D_0: VCO^+)$ and $\sigma(a^5F_1: VCO^+)$ compared to $\sigma(a^3F_2: VCO^+)$ can also be rationalized by a weak quintet-to-triplet spin-crossing mechanism. As shown by the blue line on the right side in Fig. 3, the ground electronic state symmetries of the product VCO^+ ion and the O atom are known to be $^5\Delta$ and ^3P, respectively,[37,45] and thus, the "coupled total spin" of these two products before departing may be triplet (anti-parallel), quintet (perpendicular), or septet (parallel). Therefore, the reaction system starting with either a triplet or a quintet multiplicity can proceed to the VCO^+ product channel with the same multiplicity. However, the triplet reaction system can proceed *via* a preferred triplet intermediate $[OV^+CO]$ with a relatively high reactivity while the quintet *via* a less preferred quintet intermediate $[V^+OCO]$ with a relatively low reactivity. Clearly, for the reaction system starting with a quintet multiplicity to form the preferred triplet intermediate $[OV^+CO]$, a quintet-to-triplet spin-crossing mechanism is required, and the low crossing efficiency results in a much lower reactivity of $V^+(a^5D_0)$ and $V^+(a^5F_1)$ compared to $V^+(a^3F_2)$.

Interestingly, $V^+(a^5F_1)$ exhibits the lowest reactivity for the VCO^+ product channel, even though its electronic energy is about 0.3 eV higher than that of $V^+(a^5D_0)$. This observation clearly indicates that it is not an energetic effect but a quantum electronic state effect in determining the chemical reactivity of the V^+ ion. Since both electronic states $V^+(a^5D_0$ and $a^5F_1)$ have the same electron spin, factors other than electron spin may be involved to account for this inhibition. Considering the differences in electronic configurations: $(3d)4$ for $V^+(a^5D_0)$ and $(3d)^3(4s)^1$ for $V^+(a^5F_1)$, conventional wisdom suggests that a valence electron in the 4s orbital might cause the lower reactivity of $V^+(a^5F_1)$, as the electron filled in the 4s orbital of $V^+(a^5F_1)$ may make $V^+(a^5F_1)$ more repulsive than $V^+(a^5D_0)$ when CO_2 approaches V^+ to seek bonding interaction.[46,47] A high-level theoretical calculation is called for the verification of this speculation.

As mentioned earlier, a previous study[31] of the $V^+ + CO_2$ reaction has reported the observation of enhancement of chemical reactivity when higher electron impact energies were used to prepare reactant V^+ ions. Based on similar spin-crossing mechanisms,[6–8,31] qualitative speculations about the reactivity enhancement for V^+ in excited electronic states were made. However, due to the difficulty in identifying individual electronic states, chemical reactivity measurements associated with each excited electronic state of V^+ remain unknown. Furthermore, two recent chemical kinetics studies[27,32] of the $V^+ + CO_2$ reaction at thermal energy reported no reaction for the $V^+(a^5D_J)$ ground state. The present $\sigma(a^5D_J)$ measurements disagree with the results of these kinetics studies, but are in fair agreement with those of the guided ion beam mass spectrometric study. As discussed above, the formation of product VO^+ from reaction (1) is exothermic by 0.5 eV. Thus, the observation of low $\sigma(VO^+)$ for the $V^+(a^5D_0) + CO_2$ reaction at thermal energies is expected based on the "weak spin-crossing" mechanism proposed in this study.

In addition, as depicted in Fig. 2(a)–(d), distinctive structures are observed for the $\sigma(a^5D_0$: $VO^+)$, $\sigma(a^5F_1$: $VO^+)$, and $\sigma(a^3F_2$: $VO^+)$ as well as the $\sigma(a^5D_0$: $VCO^+)$, $\sigma(a^5F_1$: $VCO^+)$ and $\sigma(a^3F_2$: $VCO^+)$ curves. This observation can also be taken as a strong piece of evidence that these σ curves result from quantum electronic state effects. Furthermore, as shown in Fig. 2(c) and (d), the E_{cm} onsets for $\sigma(a^5D_0$: $VCO^+)$, $\sigma(a^5F_1$: $VCO^+)$ and $\sigma(a^3F_2$: $VCO^+)$ are determined to be 4.1 ± 0.1, 3.8 ± 0.1, and 3.0 ± 0.1 eV, respectively. These values are consistent with the current observed thermochemical thresholds of 4.3 ± 0.1, 4.0 ± 0.1, and 3.2 ± 0.1 eV, respectively. These results again corroborate that the present experimental scheme can prepare reactant TMCs in single quantum electronic states with well-defined E_{cm} for chemical reactivity studies.

Kinetic energy dependence

As shown in Fig. 2(a), the $\sigma(a^3F_2$: $VO^+)$ curve exhibits a typical E_{cm} dependence for barrierless exothermic ion–molecule reaction channels: the higher the E_{cm}, the lower the σ value, which has been predicted by the Langevin–Gioumousis–Stevenson (LGS) capture model.[48] The calculated σ(LGS) curve scaled by a factor of 0.4 is shown as the purple dashed curve in Fig. 2(a) to compare with the experimental $\sigma(a^3F_2$: $VO^+)$ curve. The comparison reveals the general agreement of the decreasing trend observed for the $\sigma(a^3F_2$: $VO^+)$ with that predicted by the σ(LGS). We note that σ(LGS) should be compared to the sum of $\sigma(a^3F_2$: $VO^+)$ and $\sigma(a^3F_2$: $VCO^+)$ for the $V^+ + CO_2$ reaction system. However due to the fact that $\sigma(a^3F_2$: $VO^+)$ is overwhelmingly higher than $\sigma(a^3F_2$: $VCO^+)$ in the E_{cm} range of interest here, the present comparison of the $\sigma(a^3F_2$: $VO^+)$ and σ(LGS) curves is valid. As E_{cm} is increased, the smooth decrease trend of $\sigma(a^3F_2$: $VO^+)$ starts to deviate at $E_{cm} \approx$ 0.4–0.5 eV and a bump is discernible in the E_{cm} range of 0.4–4.0 eV. This bump resolved in the $\sigma(a^3F_2$: $VO^+)$ curve of Fig. 2(a) may have contributions from the excited electronic states of VO^+. More excited triplet electronic states of the product VO^+ ion are expected to become accessible at a higher E_{cm}. As pointed out above, no excited electronic state for CO is expected to be involved at excitation energies up to 6 eV measured with respect to the reactant state $V^+(a^5D_0) + CO_2(X^1\Sigma_g^+)$. Previous studies have shown that the low-lying excited triplet electronic states of VO^+, $A^3\Delta$, $B^3\Phi$, and $C^3\Pi$ are about 1.17, 1.25, and 1.87 eV higher than the $VO^+(X^3\Sigma^-)$ ground state, respectively.[31,36] Based on the thermochemical analysis, the formation of the reaction product channel $VO^+(X^3\Sigma^-) + CO(X^1\Sigma^+)$ from the reactant state $V^+(a^3F_2) + CO_2(X^1\Sigma_g^+)$ is exothermic by 1.6 eV. Therefore, $VO^+(C^3\Pi)$ becomes energetically accessible when $E_{cm} \geq$ 0.3 eV. This onset value, after taking into account the uncertainties, is consistent with the experimental onset of $E_{cm} \approx$ 0.4–0.5 eV. This agreement can also be taken as a support for the assignment that the bump originated from the formation of VO^+ in the excited electronic states including $C^3\Pi$ from $V^+(a^3F_2) + CO_2(X^1\Sigma_g^+)$.

Different from $\sigma(a^3F_2$: $VO^+)$ in Fig. 2(a), which reveals the dominant contribution from exothermic reaction product channels, the E_{cm} dependences of $\sigma(a^5D_0$: $VO^+)$ and $\sigma(a^5F_1$: $VO^+)$ in Fig. 2(b) exhibit a combined characteristic of both the exothermic and endothermic reaction product channels. As discussed above, the preferred spin-conservation rule leads to very low reactivity of both $V^+(a^5D_0$ and $a^5F_1)$ toward CO_2. As shown in Fig. 2(b), both $\sigma(a^5D_0$: $VO^+)$ and $\sigma(a^5F_1$: $VO^+)$ are found to decrease rapidly as E_{cm} is increased from 0.1 to 0.5 eV, and then they increase quickly as E_{cm} is increased from 1 eV until $E_{cm} \approx$ 4.5–5.0 eV. On the basis of thermochemical analysis, the formation of $VO^+(X^3\Sigma^-) + CO(X^1\Sigma^+)$ from $V^+(a^5D_0) + CO_2(X^1\Sigma_g^+)$ $[V^+(a^5F_1) + CO_2(X^1\Sigma_g^+)]$ is exothermic by 0.5 eV [0.8 eV]. Therefore, the $\sigma(a^5D_0$: $VO^+)$ and $\sigma(a^5F_1$: $VO^+)$ curves at $E_{cm} <$ 0.5 eV and $E_{cm} >$ 1 eV are expected to be mostly attributed to exothermic and endothermic reaction channels, respectively. Since the lowest excited electronic states of VO^+, $A^3\Delta$, is above the ground electronic state by 1.17 eV,[36] the product VO^+ can only populate in the ground electronic state for $V^+(a^5D_0)$ $[V^+(a^5F_1)]$ when $E_{cm} <$ 0.7 eV $[E_{cm} <$ 0.4 eV]. Thus, as depicted by the LGS capture model, both $\sigma(a^5D_0$: $VO^+)$ and $\sigma(a^5F_1$: $VO^+)$ are expected to decease with the increase of E_{cm} at $E_{cm} \approx$ 0.1–0.5 eV, which is consistent with the experimental observations shown in Fig. 2(b). In contrast, as E_{cm} continues to increase, more reaction paths with VO^+ populated in excited electronic states become energetically accessible, which can lead to a higher reactivity. This expectation is again in agreement with the increase of $\sigma(a^5D_0$: $VO^+)$ and $\sigma(a^5F_1$: $VO^+)$ when $E_{cm} >$ 1 eV.

In addition, it is also noted that both $\sigma(a^5D_0$: $VO^+)$ and $\sigma(a^5F_1$: $VO^+)$ are found to increase with a smaller slope at E_{cm} = 1.0–3.0 eV compared to that at E_{cm} = 3.0–4.0 eV. This observation can be explained by the different multiplicities of the product VO^+ ions formed. As discussed above, a weak quintet-to-triplet "spin-crossing" has to be involved if VO^+ is formed in the triplet electronic state for reactant V^+ ions prepared in a^5D_0 and a^5F_1, and the low crossing efficiency leads to a slower increase of $\sigma(a^5D_0$: $VO^+)$ and $\sigma(a^5F_1$: $VO^+)$ at E_{cm} = 1.0–3.0 eV. However, if VO^+ is formed in the quintet electronic state, for reaction channel (1) with V^+ in the a^5D_0 or a^5F_1 state, the reactivity is expected to be enhanced since no "spin-crossing" is required. Indeed, previous studies have shown that the two lowest quintet electronic states of VO^+,

$a^5\Sigma^-$ and $b^5\Pi$, are about 3.3 and 3.8 eV higher than the ground electronic state.[31,36] Therefore, for the $V^+ + CO_2$ reaction with V^+ prepared in the a^5D_0 or a^5F_1 state, $VO^+(a^5\Sigma^-)$ [$VO^+(b^5\Pi)$] becomes energetically accessible when $E_{cm} \geq 2.8$ or 2.5 [3.3 or 3.0] eV, which may contribute to the rapid increase of $\sigma(a^5D_0$: $VO^+)$ and $\sigma(a^5F_1$: $VO^+)$ near E_{cm} = 3.0–4.0 eV as shown in Fig. 2(b).

Furthermore, it is interesting to observe that both $\sigma(a^5D_0$: $VO^+)$ and $\sigma(a^5F_1$: $VO^+)$ reach peak values near E_{cm} = 4.0–5.0 eV and decrease sharply when $E_{cm} > 5.0$–6.0 eV. This observation can be attributed to the collision-induced dissociation (CID) of the reactant CO_2 molecule as shown in reaction (3), which has a known energetic threshold of 5.45 eV.[35] It should be noted that the CID process of reaction (3) can be achieved by further dissociation of internally excited VO^+ and VCO^+ ions, resulting in a sharp decrease of $\sigma(a^5D_0$: $VO^+)$ and $\sigma(a^5F_1$: $VO^+)$ at E_{cm} = 5.0–6.0 eV.

$$V^+(a^5D_0) + CO_2(X^1\Sigma_g^+) \rightarrow V^+(a^5D_0) + CO(X^1\Sigma^+) + O(^3P)$$
$$\Delta E = 5.45 \pm 0.12 \text{ eV} \quad (3)$$

The E_{cm} dependences of $\sigma(VCO^+)$ are depicted in Fig. 2(c) and (d). As discussed above, the formation of $VCO^+ + O$ is endothermic with reactant V^+ prepared in all three quantum electronic states: a^5D_0, a^5F_1, and a^3F_2, which is consistent with much lower $\sigma(VCO^+)$ values compared to $\sigma(VO^+)$. In Fig. 2(c), $\sigma(a^3F_2$: $VCO^+)$ exhibits a threshold position at $E_{cm} = 3.0 \pm 0.1$ eV, reaches a peak value of $\sim$0.30 Å^2 at E_{cm} = 4.5 eV, and then decreases rapidly to zero at $E_{cm} \geq 8.0$ eV. And $\sigma(a^5F_1$: $VCO^+)$ and $\sigma(a^5D_0$: $VCO^+)$ shown in Fig. 2(c) and (d) exhibit similar E_{cm} dependences to that of $\sigma(a^3F_2$: $VCO^+)$, except the difference in the peak σ values, as well as the E_{cm} threshold and the E_{cm} peak-σ position, which are found to appear at higher E_{cm} values. The E_{cm} threshold and the E_{cm} peak-σ position for $\sigma(a^5F_1$: $VCO^+)$ [$\sigma(a^5D_0$: $VCO^+)$] are observed to be 3.8 ± 0.1 and 5.2 ± 0.2 eV [4.1 ± 0.1 and 5.5 ± 0.2 eV], respectively. As pointed out earlier, the relative shifts on E_{cm} thresholds and E_{cm} peak-σ positions are consistent with the thermochemistry for this reaction channel with V^+ prepared in the three different quantum electronic states. Similar to the decrease of $\sigma(VO^+)$ at $E_{cm} > 5.0$–6.0 eV discussed above, the decrease of $\sigma(VCO^+)$ at the similar E_{cm} range can also be attributed to the CID of CO_2 as mediated by the further dissociation of the internally excited product VCO^+ ion.

Detailed comparisons between $\sigma(a^5D_0$: $VO^+)$ and $\sigma(a^5D_0$: $VCO^+)$ determined in this work and $\sigma(a^5D_J$: $VO^+)$ and $\sigma(a^5D_J$: $VCO^+)$ obtained by ref. 19 have been made as shown in Fig. 4(a) and (b), respectively. We note that in this work, the reactant V^+ ions have been prepared in the $J = 0$ spin–orbit coupled quantum electronic states with 100% purity, whereas for the measurements in ref. 19 they are expected to consist of a distribution of J-states for $\sigma(a^5D_J$: $VO^+)$ and $\sigma(a^5D_J$: $VCO^+)$. As shown in Fig. 4(a) and (b), the σ curves from both studies reveal a fair agreement with the E_{cm} dependences. However, clear differences are observed at the high $E_{cm} \geq 5.0$ eV range. More specifically, at the $E_{cm} \geq 5.0$ eV range, $\sigma(a^5D_J$: $VO^+)$ and $\sigma(a^5D_J$: $VCO^+)$ reported in ref. 19 reach the maximum values

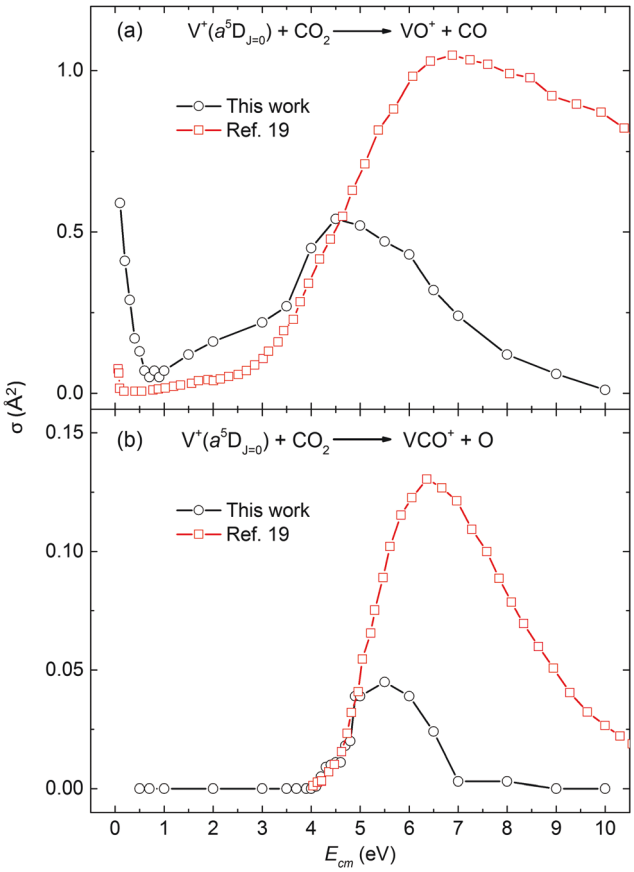

Fig. 4 Comparisons of (a) $\sigma(a^5D_0$: $VO^+)$ determined in this work with $\sigma(a^5D_J$: $VO^+)$ reported by ref. 19 and (b) $\sigma(a^5D_0$: $VCO^+)$ obtained in this work with $\sigma(a^5D_J$: $VCO^+)$ reported in ref. 19. We note that the J-levels of the a^5D_J state prepared in ref. 19 are not known.

at $\sim$7.0 and 6.5 eV, respectively, as compared to 4.5 and 5.5 eV observed in this work. The peak values of both $\sigma(a^5D_J$: $VO^+)$ and $\sigma(a^5D_J$: $VCO^+)$ reported in ref. 19 are about twice as those observed in this work. In addition, the peak values of both $\sigma(a^5D_J$: $VO^+)$ and $\sigma(a^5D_J$: $VCO^+)$ reported in ref. 19 decrease slowly, while in this work, a rapid decrease is observed. Furthermore, the $\sigma(a^5D_J$: $VO^+)$ curve at low $E_{cm} \leq 0.5$ eV observed in this work also shows different E_{cm} dependences from that reported in ref. 19. Although the detailed explanation of these discrepancies is not known, we may attribute in part to the different quantum state selections and kinetic energy resolutions for the reactant V^+ ions used in the two experiments. As shown in this work, the excited $V^+(a^3F_2)$ is much more reactive than the other two quintet states. Thus, if the V^+ ions were contaminated by $V^+(a^3F_2)$ ions, the error for σ measurements is expected to be magnified. Similarly, if the kinetic energy resolution is poor, the profile of σ as a function of E_{cm} can be dampened due to the averaging effect, which may also cause a slower decrease as observed for $\sigma(a^5D_J$: $VO^+)$ and $\sigma(a^5D_J$: $VCO^+)$.

Spin–orbit-state or *J*-state dependence

Whether J, the total angular momentum resulting from spin–orbit coupling, plays a role in the chemical reactivity of atomic

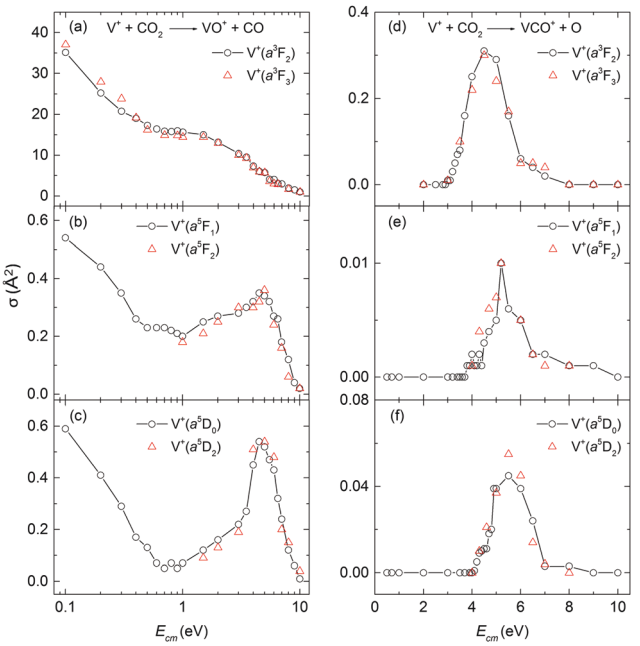

Fig. 5 Comparisons of (a) $\sigma(a^3F_2\text{: } VO^+)$ with $\sigma(a^3F_3\text{: } VO^+)$; (b) $\sigma(a^5F_1\text{: } VO^+)$ with $\sigma(a^5F_2\text{: } VO^+)$; (c) $\sigma(a^5D_0\text{: } VO^+)$ with $\sigma(a^5D_2\text{: } VO^+)$; (d) $\sigma(a^3F_2\text{: } VCO^+)$ with $\sigma(a^3F_3\text{: } VCO^+)$; (e) $\sigma(a^5F_1\text{: } VCO^+)$ with $\sigma(a^5F_2\text{: } VCO^+)$; and (f) $\sigma(a^5D_0\text{: } VCO^+)$ with $\sigma(a^5D_2\text{: } VCO^+)$ obtained in this work. These comparisons clearly show no J dependences for these integral cross section curves covering the E_{cm} range of 0.1–10.0 eV for this reaction system.

TM cations is still unclear. Experimentally, the answer to this question requires preparing TM cations in single spin–orbit coupled quantum electronic states. In this work, for each quantum electronic state of $V^+(a^5D_J)$, $V^+(a^5F_J)$, and $V^+(a^3F_J)$, we have carried out σ measurements as a function of J, in order to examine the possible spin–orbit J-state effect on the chemical reactivity of V^+ with CO_2. For the $V^+(a^5D_J)$ electronic state, we have chosen $J = 0$ and 2 for comparison. Similarly, $J = 1$ and 2 and $J = 2$ and 3 have been chosen for the $V^+(a^5F_J)$ and $V^+(a^3F_J)$ electronic states, respectively. As shown in Fig. 5(a)–(f), no J dependence is observed for all the results obtained in this work.

It should be noted that for $\sigma(a^5D_2\text{: } VO^+)$ and $\sigma(a^5F_2\text{: } VO^+)$, only measurements for $E_{cm} \geq 1.0$ eV have been performed. Considering the rest of the data shown in the same figure, the lack of data for $E_{cm} < 1.0$ eV will not affect the conclusion here: no J-state dependence has been observed in the E_{cm} range of 0.1–10.0 eV. This indicates that J of V^+ may not be conserved, or not a good quantum number for the reaction system of $V^+ + CO_2$. Instead, the electron spin of V^+ plays a dominant role, mostly favoring the conservation of the total electron spin for this reaction system. This observation indicates that spin–orbit coupling is weak and the reaction favors the conservation of total electron spins, which is consistent with the nonadiabaticity or "weak spin-crossing" mechanism discussed here for the $V^+ + CO_2$ reaction system.

Branching ratios. The detailed branching ratios (BRs) for the product channels, $VO^+ + CO$ and $VCO^+ + O$, from the reaction $V^+ + CO_2$, are listed in Table 1. Here, V^+ is prepared in each of its three spin–orbit coupled quantum electronic states, a^5D_0, a^5F_1, and a^3F_2, in the E_{cm} range from 0.1 to 10.0 eV. For all three electronic states, the $VO^+ + CO$ product channel is overwhelmingly dominant, with BRs more than 0.90 in the E_{cm} range of interest. In particular, when $E_{cm} \leq 3.0$ eV and near 10.0 eV, the $VO^+ + CO$ product channel is the only one observed. In addition, the BRs for the $VCO^+ + O$ channel for V^+ prepared in a^5D_0, a^5F_1, and a^3F_2 reach peak values of 0.09, 0.02, and 0.05 near E_{cm} = 5.5, 5.5–6.0, and 4.5–5.0 eV, respectively, and decrease quickly to a BR of 0.01 or 0.02 at both lower and higher E_{cm} directions. The detailed quantum electronic state and E_{cm}-dependences for σ and BR values obtained here are expected to be valuable benchmarks for theoretical chemical reaction dynamics studies based on first-principles calculations.

IV. Conclusion and summary

In summary, we have demonstrated that a transition metal V^+ cation can be prepared in single spin–orbit coupled quantum electronic states, a^5D_0, a^5F_1, and a^3F_2, with well-defined kinetic

Table 1 The branching ratios (BRs) of $VO^+ + CO$ and $VCO^+ + O$ reaction product channels for the reaction system of $V^+ + CO_2$ with V^+ prepared at each of its three spin–orbit coupled electronic states, a^5D_0, a^5F_1, and a^3F_2 in the E_{cm} range of 0.1–10.0 eV. We note that for all three electronic states, $VO^+ + CO$ is the only reaction product channel at $E_{cm} \leq 3.0$ eV. Therefore, this table mainly covers the BRs for the reaction at $E_{cm} \geq 3.0$ eV. The error limits of ±0.01 represent the estimated uncertainties from run-to-run independent measurements. The BRs are not listed if they are less than 0.01

	$V^+(a^5D_0) + CO_2$		$V^+(a^5F_1) + CO_2$		$V^+(a^3F_2) + CO_2$	
E_{cm} (eV)	BR(VO^+)	BR(VCO^+)	BR(VO^+)	BR(VCO^+)	BR(VO^+)	BR(VCO^+)
0.1–3.0	1.00	0.00	1.00	0.00	1.00	0.00
3.5	1.00	0.00	1.00	0.00	0.99	0.01
4.0	1.00	0.00	0.99	0.01	0.97 ± 0.01	0.03 ± 0.01
4.5	0.98 ± 0.01	0.02 ± 0.01	0.99	0.01	0.95 ± 0.01	0.05 ± 0.01
5.0	0.93 ± 0.02	0.07 ± 0.02	0.99	0.01	0.95 ± 0.01	0.05 ± 0.01
5.5	0.91 ± 0.02	0.09 ± 0.02	0.98 ± 0.01	0.02 ± 0.01	0.96 ± 0.01	0.04 ± 0.01
6.0	0.92 ± 0.02	0.08 ± 0.02	0.98 ± 0.01	0.02 ± 0.01	0.99	0.01
6.5	0.93 ± 0.02	0.07 ± 0.02	0.99	0.01	0.99	0.01
7.0	0.99	0.01	0.99	0.01	0.99	0.01
8.0	0.98 ± 0.01	0.02 ± 0.01	0.99	0.01	1.00	0.00
9.0	1.00	0.00	0.98 ± 0.01	0.02 ± 0.01	1.00	0.00
10.0	1.00	0.00	1.00	0.00	1.00	0.00

energy by utilizing a two-color laser PFI-PI detection method. Combining this quantum-state-selected V^+ PFI-PI ion source with a DQDO mass spectrometer, we have measured in detail the σ values for the reaction of $V^+ + CO_2$ as a function of both the E_{cm} and internal quantum electronic state of the V^+ ion. We observed that $V^+(a^5D_0)$ and $V^+(a^5F_1)$ exhibit a much lower chemical reactivity than $V^+(a^3F_2)$ with CO_2, which can be rationalized by a ''weak quintet-to-triplet spin-crossing'' mechanism. Since this method is readily applicable to other TM cations, the success of this experiment paves the way for detailed investigation of the role played by low-lying electronic states in the complex chemistry involving TM cations. In addition, the observation that $\sigma(a^3F_2)$ is much higher than $\sigma(a^5D_0)$ and $\sigma(a^5F_1)$ for $V^+ + CO_2$ shows that the chemical reactivity of TM cations can be greatly altered by their internal quantum electronic states, thus allowing the control of the chemical reactivity of TM cations by quantum electronic state selection.

Conflicts of interest

There are no conflicts to declare.

Acknowledgements

This work was supported by the National Science Foundation under CHE-1763319. CYN is also grateful to Dr Huie Tarng Liou for his generous donation of research support for the Ng Laboratory.

References

1 P. B. Armentrout and J. L. Beauchamp, *Acc. Chem. Res.*, 1989, **22**, 315–321.
2 L. Operti and R. Rabezzana, *Mass Spectrom. Rev.*, 2006, **25**, 483–513.
3 D. K. Böhme and H. Schwarz, *Angew. Chem., Int. Ed.*, 2005, **44**, 2336–2354.
4 E. Harris, B. Sinha, D. van Pinxteren, A. Tilgner, K. W. Fomba, J. Schneider, A. Roth, T. Gnauk, B. Fahlbusch, S. Mertes, T. Lee, J. Collett, S. Foley, S. Borrmann, P. Hoppe and H. Herrmann, *Science*, 2013, **340**, 727–730.
5 A. Veillard, *Quantum Chemistry: The Challenge of Transition Metals and Coordination Chemistry*, Springer, Netherlands, 2012.
6 P. Armentrout, *Annu. Rev. Phys. Chem.*, 1990, **41**, 313–344.
7 J. C. Weisshaar, in *Advances in Chemical Physics: State-Selected and State-To-State Ion-Molecule Reaction Dynamics, Part 1. Experiment*, ed. C. Y. Ng and M. Baer, John Wiley & Sons, Inc., 1992, vol. 82, pp. 213–262.
8 D. Schröder, S. Shaik and H. Schwarz, *Acc. Chem. Res.*, 2000, **33**, 139–145.
9 C. Y. Ng, *J. Phys. Chem. A*, 2002, **106**, 5953–5966.
10 S. Willitsch, M. T. Bell, A. D. Gingell, S. R. Procter and T. P. Softley, *Phys. Rev. Lett.*, 2008, **100**, 043203.
11 K. Okada, T. Suganuma, T. Furukawa, T. Takayanagi, M. Wada and H. A. Schuessler, *Phys. Rev. A: At., Mol., Opt. Phys.*, 2013, **87**, 043427.
12 B. Xiong, *PhD dissertation*, University of California, Davis, 2017.
13 Y. C. Chang, B. Xiong, Y. Xu and C. Y. Ng, *J. Phys. Chem. A*, 2019, DOI: 10.1021/acs.jpca.9b00511.
14 Y. C. Chang, H. Xu, Y. Xu, Z. Lu, Y. H. Chiu, D. J. Levandier and C. Y. Ng, *J. Chem. Phys.*, 2011, **134**, 201105.
15 Y. C. Chang, Y. Xu, Z. Lu, H. Xu and C. Y. Ng, *J. Chem. Phys.*, 2012, **137**, 104202.
16 Y. Xu, Y. C. Chang, Z. Lu and C. Ng, *Astrophys. J.*, 2013, **769**, 72.
17 Y. Xu, B. Xiong, Y. C. Chang and C. Ng, *Astrophys. J.*, 2016, **827**, 17.
18 Y. Xu, B. Xiong, Y. C. Chang and C. Y. Ng, *J. Phys. Chem. A*, 2018, **122**, 6491–6499.
19 Y. Xu, B. Xiong, Y. C. Chang and C. Y. Ng, *J. Chem. Phys.*, 2012, **137**, 241101.
20 Y. Xu, B. Xiong, Y. C. Chang and C. Y. Ng, *J. Chem. Phys.*, 2013, **139**, 024203.
21 Y. Xu, B. Xiong, Y. C. Chang, Y. Pan, P. K. Lo, K. C. Lau and C. Y. Ng, *Phys. Chem. Chem. Phys.*, 2017, **19**, 9778–9789.
22 Y. Xu, B. Xiong, Y. C. Chang and C. Y. Ng, *Astrophys. J.*, 2018, **861**, 17.
23 B. Xiong, Y. C. Chang and C. Y. Ng, *Phys. Chem. Chem. Phys.*, 2017, **19**, 18619–18627.
24 B. Xiong, Y. C. Chang and C. Y. Ng, *Phys. Chem. Chem. Phys.*, 2017, **19**, 29057–29067.
25 E. U. Condon, E. U. Condon and G. H. Shortley, *The Theory of Atomic Spectra*, Cambridge University Press, 1951.
26 J. L. Elkind and P. B. Armentrout, *J. Phys. Chem.*, 1985, **89**, 5626–5636.
27 G. K. Koyanagi and D. K. Bohme, *J. Phys. Chem. A*, 2006, **110**, 1232–1241.
28 S. L. Suib, *New and Future Developments in Catalysis: Activation of Carbon Dioxide*, Elsevier Science, 2013.
29 D. Y. Leung, G. Caramanna and M. M. Maroto-Valer, *Renewable Sustainable Energy Rev.*, 2014, **39**, 426–443.
30 M. M. Kappes and R. H. Staley, *J. Phys. Chem.*, 1981, **85**, 942–944.
31 M. Sievers and P. B. Armentrout, *J. Chem. Phys.*, 1995, **102**, 754–762.
32 J. Herman, J. D. Foutch and G. E. Davico, *J. Phys. Chem. A*, 2007, **111**, 2461–2468.
33 P. J. Chantry, *J. Chem. Phys.*, 1971, **55**, 2746–2759.
34 M. W. Chase Jr, *J. Phys. Chem. Ref. Data, Monogr.*, 1998, **9**, 1922.
35 R. Branko, E. P. Reinhardt, L. Gregor von, K. Deepti, B. Alexander, L. David, M. David and F. W. Albert, *J. Phys.: Conf. Ser.*, 2005, **16**, 561.
36 J. M. Dyke, B. W. J. Gravenor, M. P. Hastings and A. Morris, *J. Phys. Chem.*, 1985, **89**, 4613–4617.
37 J. E. Sansonetti and W. C. Martin, *J. Phys. Chem. Ref. Data*, 2005, **34**, 1559–2259.
38 A. G. Middleton, M. J. Brunger and P. J. O. Teubner, *J. Phys. B: At., Mol. Opt. Phys.*, 1993, **26**, 1743.
39 E. Wigner and E. Witmer, *Z. Phys.*, 1928, **51**, 859.

40 Z. Luo, Y. C. Chang, H. Huang and C. Y. Ng, *J. Phys. Chem. A*, 2015, **119**, 11162–11169.
41 E. A. Carter and W. A. Goddard, *J. Phys. Chem.*, 1988, **92**, 2109–2115.
42 E. Miliordos and A. Mavridis, *J. Phys. Chem. A*, 2007, **111**, 1953–1965.
43 M. Sodupe, V. Branchadell, M. Rosi and C. W. Bauschlicher, *J. Phys. Chem. A*, 1997, **101**, 7854–7859.
44 H. Schwarz, *Int. J. Mass Spectrom.*, 2004, **237**, 75–105.
45 N. E. Schultz, Y. Zhao and D. G. Truhlar, *J. Phys. Chem. A*, 2005, **109**, 11127–11143.
46 J. L. Elkind and P. B. Armentrout, *J. Phys. Chem.*, 1987, **91**, 2037–2045.
47 J. C. Weisshaar, *Acc. Chem. Res.*, 1993, **26**, 213–219.
48 G. Gioumousis and D. Stevenson, *J. Chem. Phys.*, 1958, **29**, 294–299.